CARLOTO, I., JOHNSTON, P., PESTANA, C.J. and LAWTON, L.A. 2021. Detection of morphological changes caused by chemical stress in the cyanobacterium Planktothrix agardhii using convolutional neural networks. *Science of the total environment* [online], 784, article 146956. Available from: https://doi.org/10.1016/j.scitotenv.2021.146956

# Detection of morphological changes caused by chemical stress in the cyanobacterium Planktothrix agardhii using convolutional neural networks.

CARLOTO, I., JOHNSTON, P., PESTANA, C.J. and LAWTON, L.A.

2021

Science of the Total Environment 784 (2021) 146956

Contents lists available at ScienceDirect

Science of the Total Environment

journal homepage: www.elsevier.com/locate/scitotenv

# Detection of morphological changes caused by chemical stress in the cyanobacterium *Planktothrix agardhii* using convolutional neural networks

Ismael Carloto [a,*], Pamela Johnston [b], Carlos J. Pestana [a], Linda A. Lawton [a]

[a] School of Pharmacy and Life Sciences, Robert Gordon University, Garthdee Road, Aberdeen AB10 7GJ, UK
[b] School of Computing, Robert Gordon University, Garthdee Road, Aberdeen AB10 7GJ, UK

## HIGHLIGHTS

- GrabCut processing boosts accuracy for morphological change detection on *P. agardhii*.
- Adam and RMSProp optimizers enhance accuracy for trichome classification.
- Trichome classification can be tackled with a limited number of learned features.
- Method based on image recognition can be used to ensure water safety globally.

## GRAPHICAL ABSTRACT

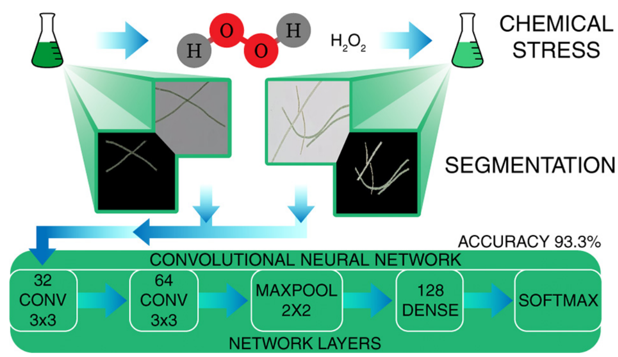


## ARTICLE INFO

*Article history:*
Received 23 November 2020
Received in revised form 31 March 2021
Accepted 31 March 2021
Available online 7 April 2021

Editor: Charlotte Poschenrieder

*Keywords:*
Cyanobacteria
CNN
Water treatment
Hydrogen peroxide
Image recognition
Image segmentation

## ABSTRACT

The presence of harmful algal bloom in many reservoirs around the world, alongside the lack of sanitation law/ordinance regarding cyanotoxin monitoring (particularly in developing countries), create a scenario in which the local population could potentially chronically consume cyanotoxin-contaminated waters. Therefore, it is crucial to develop low cost tools to detect possible systems failures and consequent toxin release inferred by morphological changes of cyanobacteria in the raw water. This paper aimed to look for the best combination of convolutional neural network (CNN), optimizer and image segmentation technique to differentiate *P. agardhii* trichomes before and after chemical stress caused by the addition of hydrogen peroxide. This method takes a step towards accurate monitoring of cyanobacteria in the field without the need for a mobile lab. After testing three different network architectures (AlexNet, 3ConvLayer and 2ConvLayer), four different optimizers (Adam, Adagrad, RMSProp and SDG) and five different image segmentations methods (Canny Edge Detection, Morphological Filter, HP filter, GrabCut and Watershed), the combination 2ConvLayer with Adam optimizer and GrabCut segmentation, provided the highest median accuracy (93.33%) for identifying $H_2O_2$-induced morphological changes in *P. agardhii*. Our results emphasize the fact that the trichome classification problem can be adequately tackled with a limited number of learned features due to the lack of complexity in micrographs from before and after chemical stress. To the authors' knowledge, this is the first time that CNNs were applied to detect morphological changes in cyanobacteria caused by chemical stress. Thus, it is a significant step forward in developing low cost tools based on image recognition, to shield water consumers, especially in the poorest regions, against cyanotoxin-contaminated water.



* Corresponding author.
*E-mail addresses:* ismael.lopes@ifce.edu.br (I. Carloto), p.johnston2@rgu.ac.uk (P. Johnston), c.pestana@rgu.ac.uk (C.J. Pestana), l.lawton@rgu.ac.uk (L.A. Lawton).

https://doi.org/10.1016/j.scitotenv.2021.146956
0048-9697/

## 1. Introduction

Due to climatic conditions and inadequate sanitation systems, reservoirs in many tropical and developing countries are eutrophic and have become favourable environments for harmful cyanobacterial blooms (Barros et al., 2017; Carloto et al., 2015). Among harmful cyanobacteria, *Planktothrix* has been identified as a dominant bloom-forming genus, as well as a frequent toxin producer (Huisman et al., 2018). Many oxidation-based treatment methods have been proposed for use in water treatment plants (WTPs) (Steynberg et al., 1996; Chen et al., 2009; Jian et al., 2019), and within reservoirs (Bauzá et al., 2014; Matthijs et al., 2012; Wang et al., 2012; Barrington and Ghadouani, 2008; Zhou et al., 2018) to control phytoplankton. Hydrogen peroxide ($H_2O_2$) has been demonstrated as a suitable in-reservoir solution due to being a strong oxidant, selective against cyanobacteria and lack of toxic by-product formation (Drabkova et al., 2007; Yang et al., 2018). Although addition of $H_2O_2$ can significantly reduce the cell density of cyanobacteria, it can also cause cell lysis/damage, possibly releasing toxins into the surrounding water (Westrick et al., 2010; Pietsch et al., 2002; Daly et al., 2007; Zamyadi et al., 2010; Hobson et al., 2012; Huo et al., 2015; Fan et al., 2013, 2014). Thus, a warning system to alert operators to potential toxin release is needed. Image recognition could provide this tool. Convolutional Neural Networks (CNN) are the most successful method used for pattern recognition in images (Sarigul et al., 2019). CNN roughly mimic the visual cortex of humans and are characterized by a successful hierarchical object recognition system which extracts localized features from input images, enabling classification of the output (Ciresan et al., n.d.). Outputs can be enhanced by image segmentation as a pre-processing step (Tang et al., 2018). Image segmentation divides a given image into different regions, aiding localization of objects and object boundaries (Cheng et al., 2001; Ying, 2016). Recently, many studies have reported on the use of CNN for phytoplankton recognition (Pedraza et al., 2017; Zheng et al., 2017; Li et al., 2017; Dunker et al., 2018; Park et al., 2019; Baeka et al., 2020; Panta et al., 2020; Qian et al., 2020), however, this is the first study using CNN to detect morphological changes in filamentous cyanobacteria caused by chemical stress. The current study elucidates the effectiveness of CNN for the detection of trichome breakage caused by chemical stress through (i) finding the most suitable segmentation method; and (ii) determining the best CNN architecture for *Planktothrix agardhii* recognition before and after the addition of $H_2O_2$.

## 2. Materials and methods

### 2.1. Cyanobacteria culture and enumeration

Axenic *Planktothrix agardhii* CCNP 1305 culture was incubated in BG-11 (Rippka et al., 1979) medium at 20 ± 1 °C with 12 h/12 h light/dark cycle under cool white fluorescent light with an intensity of 20 μmol photons $m^{-2}$ $s^{-1}$. Cell density was estimated using an Olympus microscope (Model BX53M), with a Sedgewick-Rafter chamber at 200× magnification.

### 2.2. Oxidation of P. agardhii CCNP 1305 with hydrogen peroxide

In order to train a CNN in recognising the morphological changes in *P. agardhii* CCNP 1305 it was necessary both to choose a chemical compound and determine its ideal concentration that induces morphological changes rather than complete destruction of the organisms. Since $H_2O_2$ has been known as damage-causing compound in cyanobacteria cells (Latifi et al., 2009), used to a great extent as cyanobacterial blooms suppression (Matthijs et al., 2012; Matthijs et al., 2016) and as a peroxidation compound in water treatment plants (Wang et al., 2018), it was the chosen compound to perform the experiments. To find the optimum $H_2O_2$ concentration three batch-type experiments were performed. Hydrogen peroxide was added to *P. agardhii* CCNP 1305 cell suspension (SM Table S1) to achieve final concentrations of 5, 10, 15, 20 mg $L^{-1}$ in 40 mL of $H_2O_2$. A second experiment was carried out with three different concentrations of 30, 40 and 80 mg $L^{-1}$ $H_2O_2$. Finally, a third, confirmatory, study was performed repeating concentrations 40 and 80 mg $L^{-1}$ $H_2O_2$. In all experiments *P. agardhii* CCNP 1305 cultures were exposed to $H_2O_2$ with a contact time of 24 h at 20 ± 1 °C and constant cool white fluorescent light with 40 μmol photons $m^{-2}$ $s^{-1}$ intensity. Samples were taken before the addition of $H_2O_2$ and after 0.5, 1, 3, 6 and 24 h. Flask for each concentration were prepared in triplicate.

### 2.3. Image acquisition and image dataset

The RGB (Red, Green, Blue) images were captured using a YenCam HD (Yenway Microscopes) camera at 500× magnification and a resolution of 1920 × 1080 pixels. Different points of the microscope slides were randomly selected to capture the images, in order to ensure that no *P. agardhii* trichome was captured more than once. The acquired images were saved in PNG format. Images of *P. agardhii* CCNP 1305 were captured before and after hydrogen peroxide addition. Many images contained multiple trichomes, and no manual attempt was made to isolate individual organisms from other organisms or background. The final dataset of original images consisted of 2099 images before, and 2099 for each sampling point after the application of the given $H_2O_2$ concentrations.

### 2.4. Hardware and software

The CNN models were implemented using Keras/TensorFlow python libraries, on an Omen Hp laptop with 16GB RAM (HP Inc., USA), Intel Core i7 2.6 GHz central processing unit and equipped with a NVIDIA GeForce RTX 2060 graphics card.

### 2.5. Image processing

All images were resized from their original size of 1920 × 1080 to either 128 × 128 pixels for the smallest CNN architecture or 224 × 224 pixels for the larger architectures. Reducing the size of the raw images reduces and distorts finer details but maintains the overall image and the overall shape of the trichomes. All images were also normalized, which is a common procedure in image pre-processing that changes the range of each pixel intensity value.

In the first instance, no image pre-processing was applied (From now on called None), and the resized and normalized RGB images were passed straight to the CNN. Thereafter, image refinement was performed using five different methods: high pass filtering; Canny edge detection (Canny, 1986); GrabCut (Rother et al., 2004); Watershed (Meyer, 1992) and morphological mask image segmentation.

### 2.6. Convolutional neural networks for cyanobacteria recognition

In order to determine a suitable CNN architecture three different architectures were tested: one simple architecture loosely based on LeNet5 (LeCun et al., 1998), from now on called 3ConvLayer, a variation on AlexNet (Krizhevsky et al., 2012) and one based on a Keras implementation which is known to achieve 99.25% accuracy on MNIST (LeCun et al., 1998), from now on called 2ConvLayer. The MNIST dataset consists of greyscale images of handwritten digits. MNIST is relevant because classification of MNIST digits relies solely on the shape of the digits as no texture is present. Trichomes exposed to $H_2O_2$ adopt distinctive shapes which might prove to be a suitably discriminative feature for classification.

The descriptions use the following notations: conv*n*x*n*-*m* means a convolutional layer with a *n*x*n* kernel size and *m* filters; maxpool*n*x*n* means a max pooling layer, fc-*n* means a fully connected dense layer with *n* nodes. All networks use Rectified Linear Units (ReLU) activations.

LeNet5 is an old CNN architecture first applied to the recognition of handwritten digits (Canny, 1986). It is known to be able to classify small, simple images based on the shapes depicted in them. The architecture of our 3ConvLayer was: conv3x3-32, conv3x3-32, conv3x3-32, fc-64, softmax. 3ConvLayer has ~30.5 million trainable parameters with no dropout.

AlexNet (Krizhevsky et al., 2012) was a CNN designed to tackle the ImageNet dataset of real-world images (Deng et al., 2009). Our variation architecture is: conv11x11-96, maxpool2x2, conv11x11-256, maxpool2x2, conv3x3-384, conv3x3-384, conv3x3-256, maxpool2x2, fc-4096, fc-4096, fc-1000, softmax. The network also uses batch normalization to allow training of such a deep neural network and dropout of 40% in the fully connected layers. Input image size was $224 \times 224$. The use of large kernels in the early layers of this model investigates whether other features, such as texture can be learned from the present dataset and enhance classification accuracy. This model was the deepest model in our tests and has ~28 million trainable parameters.

The third CNN model consists of conv3x3-32, conv3x3-64, maxpool, dense-128, softmax. The input image size for this model was $224 \times 224$, and the stride of the first layer was 4. Dropout of 50% was applied to the dense layer only. 2ConvLayer has just under 24 million trainable parameters. Compared with our AlexNet variation, it is a shallow but wide network.

### 2.7. Selection of optimizers

In order to obtain a high level of classification accuracy, the neural network architecture and the dataset must be matched with an appropriate method of optimization for training. In a neural network, the sample data is passed through the neural network and a predicted classification is calculated. The difference between the classification predicted by the network and actual classification is called the loss. The loss is then back propagated through the network and used to alter the network's internal parameters so that the loss is minimised. The optimizer ultimately controls how the loss is used to change the internal network parameters during training. The different optimizers tested here are: Stochastic Gradient Descent (SGD) (Chung, 1954); RMSProp (Tieleman and Hinton, 2012); Adagrad (Duchi et al., 2011); and Adam (Kingma and Ba, 2014). Of these, SGD is the only non-adaptive optimiser. Adaptive optimisers base the weight change on current and previous values and often allow neural networks to converge faster and produce more accurate results.

### 2.8. Statistical analysis

Three different CNN architectures with four different optimizers on image datasets that were pre-processed in six different ways were tested. Randomisation was inherent in the initial configuration of our CNNs as was allocation of images to test/train sets. Since the used dataset is perfectly balanced (2099 before/2099 after $H_2O_2$ exposure), accuracy rate was used as performance evaluation index (Galar et al., 2012). Statistical analysis was performed in order to ascertain the optimal architecture/optimizer/image pre-processing combination. The Shapiro-Wilk normality test was performed for each analysed parameter to determine the data distribution type (significance level of 5%). According to the result, parametric or non-parametric tests were utilized to compare the parameters. To test the significance of difference between different combinations of experimental parameters, nonparametric Kruskal-Wallis (KW) and one-tailed Pairwise Wilcoxon rank-sum (PW) tests (with Bonferroni) were applied (5% significance level). All statistical analyses were performed in RStudio.

## 3. Results and discussion

### 3.1. P. agardhii CCNP 1305 trichome breakage caused by the addition of $H_2O_2$

Morphological changes for all $H_2O_2$ concentrations were verified by microscopy (Fig. 1). No changes were observed for 5, 10, 15, 20 mg $L^{-1}$ $H_2O_2$ for any sample over the contact time (SM Figs. S1–S4). As no morphological changes were observed initially, three higher concentrations of $H_2O_2$ (30, 40 and 80 mg $L^{-1}$) were applied. Here no trichome alteration was detected for 30 mg $L^{-1}$ (SM Fig. S5), however, from 1 h onwards, complete destruction of the trichomes was observed for samples treated with 40 mg $L^{-1}$ $H_2O_2$ (SM Fig. S6). Surprisingly, no breakage of trichomes was observed before 6 h with 80 mg $L^{-1}$ $H_2O_2$(SM Figs. S7–S8).

Additionally, colour changes and intracellular content release were observed.

A confirmatory experiment was carried out (40 mg $L^{-1}$ and 80 mg $L^{-1}$). Complete destruction of the trichomes in samples treated with 40 mg $L^{-1}$ $H_2O_2$ was observed again, but only from 3 h onwards (SM Fig. S9). In samples treated with 80 mg $L^{-1}$ $H_2O_2$ trichome breakage was only observed after 24 h of $H_2O_2$ addition (SM Figs. S10–S11). Ultimately, it was decided to use 80 mg $L^{-1}$ $H_2O_2$ (SM Fig. S7) to induce morphological changes in *P. agardhii* CCNP 1305 to create the library of "after treatment" images to train the CNN.

### 3.2. Image process methods

#### 3.2.1. Image segmentation outcomes

The high pass filter method applied a discrete Fourier transformation to the normalized, greyscale image then used a high pass filter to smooth low frequency background pixels. The pixels were then segmented based on a threshold derived from their mean and variance (SM Fig. S12). For GrabCut, a border round the edge of the image was labelled "definite background". Since the majority of the trichome pixels are in the central portion of the images, this was sufficient to segment slide background from trichome (SM Fig. S13). The morphological filter used a mask created by thresholding the image based on Otsu's thresholding (Otsu, 1979), to create a rough trichome/background segmentation. The mask was then refined using erosion with a $3 \times 3$ kernel to remove noise, followed by dilation to ensure all relevant trichome pixels were captured (SM Fig. S14).

Image refinement suppressed pixels that were irrelevant to image classification by setting them to zero. The high pass filtered background suppression left the trichome shape intact with a clearly visible border of surrounding background pixels (Fig. 2).

The Canny filter revealed some noise surrounding the trichomes that is invisible in the unprocessed images. GrabCut provided neat segmentation, but some potential noise in the background passes through and some spatially close trichomes were completely connected by background sections. The morphological mask removed all noise but removed some trichomes as well.

All forms of image segmentation and background suppression were performed prior to resizing and normalization, except for GrabCut, where the images were resized prior to applying the algorithm to reduce processing time. OpenCV was used for image pre-processing.

#### 3.2.2. Comparison of architecture performance

To determine the most suitable configuration for detection of morphological changes, all architectures were run with and without segmentation techniques, as well as four different optimizers, resulting in a total 432 runs (each combination was run 10, 25 and 30 epochs twice) (SM Table S2). The overall accuracy was determined (Table 1). To compare the results of all possible combinations of parameters, the distribution of the accuracy data was determined by the SW test. The distribution of accuracy data (AlexNet: *p*-value: 9.64 $10^{-9}$; 3ConvLayer: p-value: 7.51 $10^{-15}$ and 2ConvLayer: p-value: 6.13 $10^{-10}$) were significantly different ($p < 0.05$) from normal distribution, thus, the median was chosen as a measure of central tendency.

In 31 out of 432 of all combinations, accuracies ≥90% were achieved. Although the highest accuracy (95.4%) was achieved in AlexNet after 30 epochs, and 3ConvLayer after 25 epochs, 2ConvLayer achieved better results when considering the median accuracy (76.5%) of all applied combinations. The median value of 3ConvLayer accuracy was 53.6%,

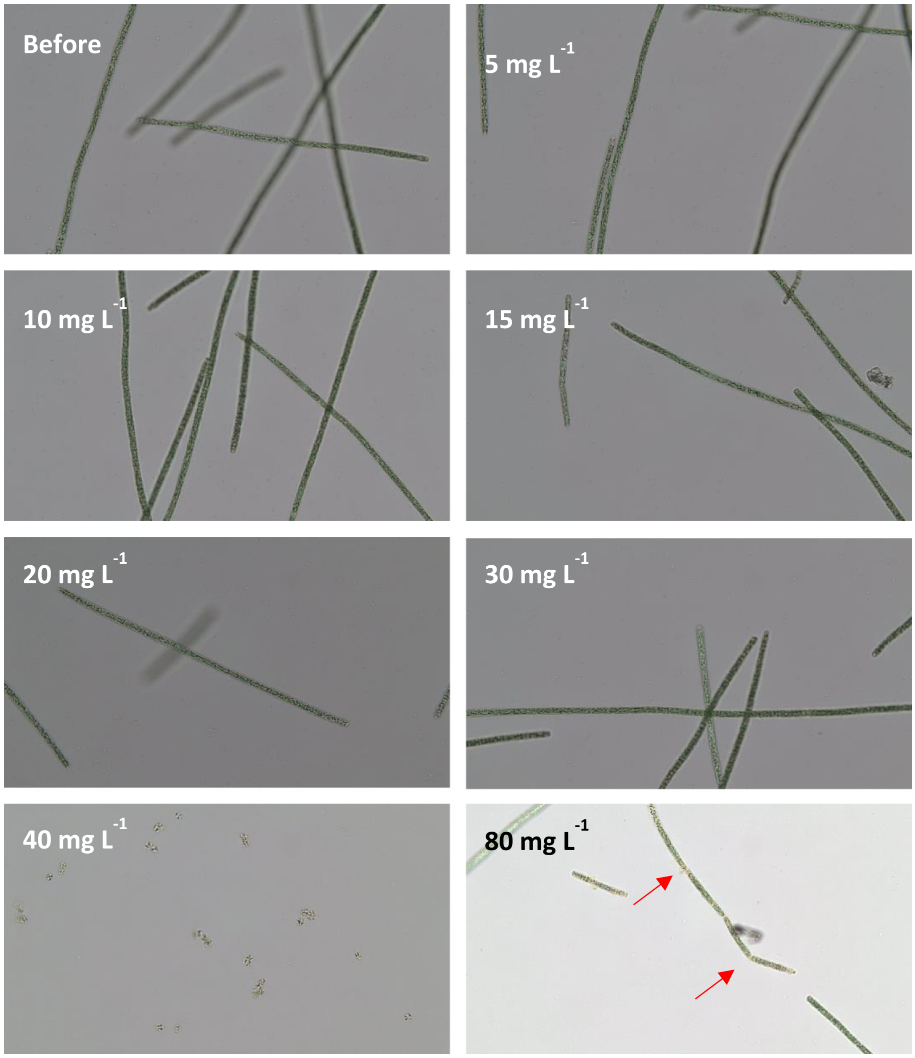


**Fig. 1.** Effect of all analysed concentrations of $H_2O_2$ on *P. agardhii* CCNP 1305 trichomes after 6 h contact time (Magnification 500×). Red arrows indicate trichome breakage. (For interpretation of the references to colour in this figure legend, the reader is referred to the web version of this article.)

while for AlexNet it was 67.7%. Of the 31 combinations that achieved an accuracy of >90%, 13 were achieved by 2ConvLayer and nine each by AlexNet and 3ConvLayer.

The Kruskal-Wallis test (KW), followed by Pairwise Wilcoxon signed-rank (PW) test were performed. There was a significant difference in accuracy among the architectures (KW p-value: 6.3 $10^{-8}$). Further, the accuracies of 3ConvLayer were different from both AlexNet (PW p-value: 1.9 $10^{-5}$) and 2ConvLayer (3.6 $10^{-7}$), while 2ConvLayer and AlexNet were statistically the same (p-value: 0.07).

The deeper AlexNet variation would theoretically allow for more complicated shapes and inter- and intra-class variation (Krizhevsky et al., 2012). The trichomes themselves do not exhibit such complexity, therefore the depth of AlexNet is not an advantage for their classification. The higher number of parameters in the largely convolutional 3ConvLayer network means that it fails to converge or converges more poorly more frequently than the others. The 2ConvLayer architecture contains fewer convolutional layers than the others and the fewest trainable parameters of all. The fact that it has the best overall performance implies that the trichome classification problem can be adequately tackled with fewer learned features.

### 3.2.3. Comparison of image segmentation performance

For all combinations of network architectures and optimizers, the median value for accuracy was 50.0%, when no data segmentation method was utilized (Fig. 3A), meaning that the networks were not able to learn any pattern. On the other hand, even without image segmentation, 2ConvLayer network with the RMSProp and with the Adam optimizers (after 30 epochs respectively) accuracies of 91.6% and 90.9% respectively were achieved.

The median accuracy for the Watershed optimizer was 51.7%. Out of 72 runs performed with all networks 30 achieved an accuracy of 50.0%, similar to running the network without any data segmentation. When combining the 2ConvLayer network with the Adam optimizer an accuracy of 92.8% (25 epochs) was achieved. Canny Edge achieved a median accuracy of 62.6%. The HP and Morphological Filters achieved median accuracies of 81.8% and 82.4%, respectively. The maximum accuracies were reached with 3ConvLayer for HP filter (with Adam) and AlexNet (with RMSProp) for morphological filter at 88.7% each. While the GrabCut segmentation had a median accuracy of 86.2%, achieving maximum accuracy of 95.4% with AlexNet and the Adagrad optimizer (30 epochs). Out of 72 runs performed with the GrabCut segmented dataset 28 (40%) achieved ≥90.0%.

The KW and PW tests determined a significant difference in accuracy by applying data segmentation (*p*-value: 2.2 $10^{-16}$, results of PW test in SM Table S3).

Only the HP and Morphological Filters were not statistically different. Although there is a difference between the Watershed segmentation and the runs without data segmentation, the p-value was the

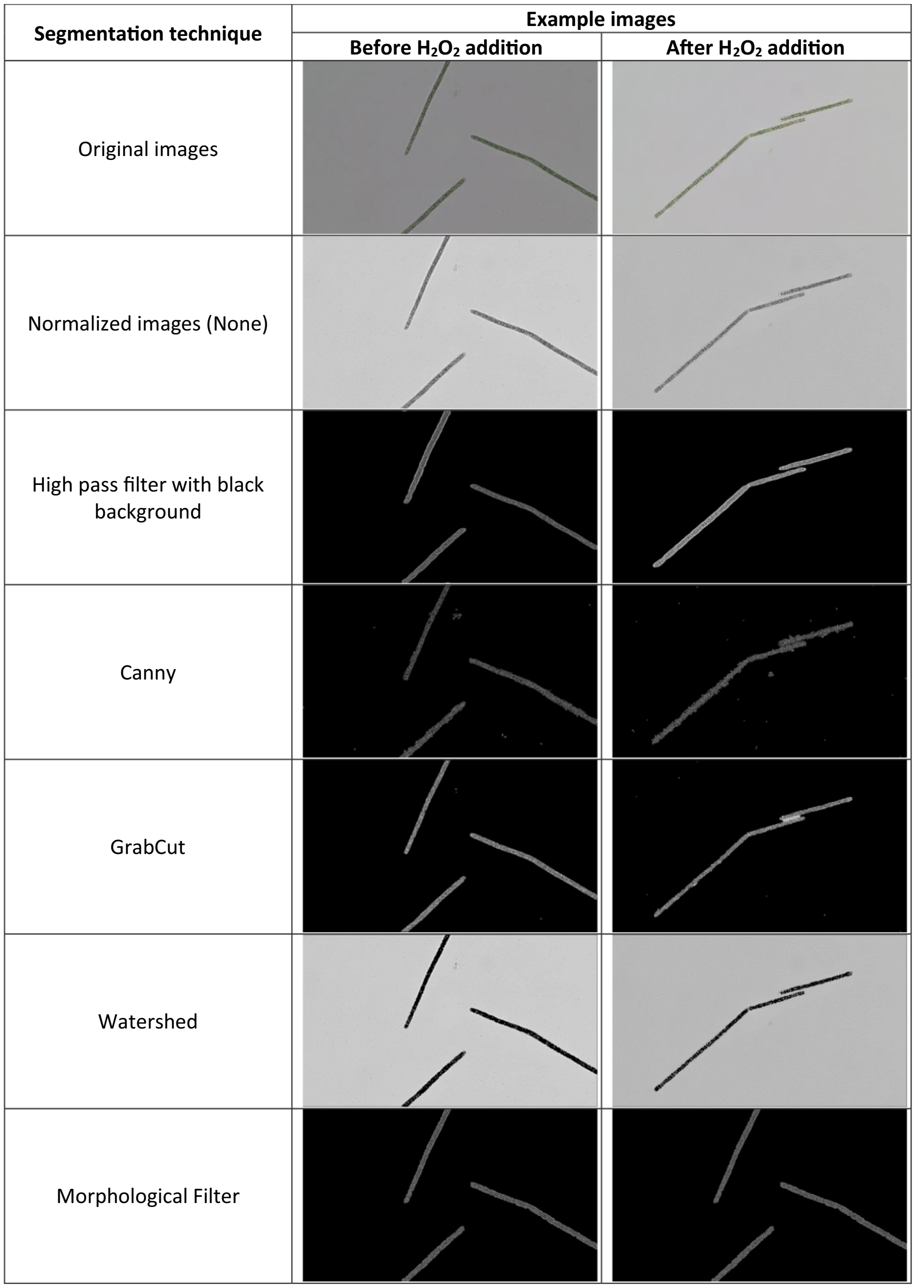


**Fig. 2.** Effect of 80 mg $L^{-1}$ $H_2O_2$ addition on trichomes of *P. agardhii* CCPN 1305 after 6 h, magnification 500×. Effect is visualized by application of different segmentation techniques on the micrograph.

closest to significance level of 5%. Therefore, Watershed segmentation was the least effective pre-processing method and GrabCut the most. Thus, suppressing background pixels in images by setting them to zero is a valid technique for enhancing CNN accuracy and reproducibility. Since GrabCut was the only pre-processing technique that resized the images before applying the filter, images can be validly resized prior to processing without substantial loss in classification accuracy.

### 3.2.4. Comparison of optimizers

When the Adam optimizer was used the median value of accuracy was 80.8%, the highest of all optimizers (Fig. 3B). For RMSProp, the median accuracy was 78.7%, while for SGD and Adagrad median accuracies were 56.3% and 51.0%, respectively. There was a significant difference between accuracies (KW $p$-value: 5.2 $10^{-9}$). There was no significant difference between Adam and RMSProp or between Adagrad and SGD (PW test results in SM Table S4). The adaptive optimizers RMSProp and Adam performed better than SGD. Thus, the intra-class variation in the present image dataset as interpreted by the two shallower networks is relatively small, leaving Adagrad with little advantage over SGD.

### 3.2.5. Overall evaluation of combinations of architecture, segmentation and optimizer

2ConvLayer and AlexNet were the best performing architectures, GrabCut was the highest performing segmentation technique and Adam and RMSProp were the best optimizers tested. To determine the best combination of architecture, segmentation and optimizer statistical analysis was employed (Fig. 4).

For AlexNet, the highest median accuracy was achieved with GrabCut (88.1%), followed by Morphological Filter (81.7%). Using images without segmentation or using Watershed segmentation, the network cannot be trained, reaching median accuracies of 50.0% and 55.5%, respectively.

**Table 1**
Overall accuracy results, for architectures and segmentation. Bold values represent the highest value of accuracy achieved for median and maximum values.

| Architecture | Segmentation | Median | Max | SD | Count |
|---|---|---|---|---|---|
| 2ConvLayer | Canny | 0.712 | 0.849 | 0.116 | 24 |
| 2ConvLayer | GrabCut | 0.861 | 0.933 | 0.169 | 24 |
| 2ConvLayer | Hp filter | 0.837 | 0.859 | 0.146 | 24 |
| 2ConvLayer | Morph. filter | 0.849 | 0.878 | 0.133 | 24 |
| 2ConvLayer | None | 0.574 | 0.916 | 0.149 | 24 |
| 2ConvLayer | Watershed | 0.648 | 0.928 | 0.146 | 24 |
| 3ConvLayer | Canny | 0.557 | 0.684 | 0.053 | 24 |
| 3ConvLayer | GrabCut | 0.713 | 0.945 | 0.202 | 24 |
| 3ConvLayer | Hp filter | 0.717 | 0.887 | 0.166 | 24 |
| 3ConvLayer | Morph. filter | 0.563 | 0.88 | 0.165 | 24 |
| 3ConvLayer | None | 0.500 | 0.677 | 0.058 | 24 |
| 3ConvLayer | Watershed | 0.500 | 0.665 | 0.054 | 24 |
| AlexNet | Canny | 0.649 | 0.818 | 0.096 | 24 |
| AlexNet | GrabCut | **0.880** | **0.954** | 0.153 | 24 |
| AlexNet | Hp filter | 0.809 | 0.854 | 0.131 | 24 |
| AlexNet | Morph. filter | 0.817 | 0.887 | 0.131 | 24 |
| AlexNet | None | 0.500 | 0.694 | 0.058 | 24 |
| AlexNet | Watershed | 0.554 | 0.849 | 0.100 | 24 |

SD = Standard Deviation; Count = Total of runs performed with a combination of architecture and image segmentation in each line.

There were significant statistical differences between image segmentation methods (KW *p*-value: 5.19 $10^{-12}$, PW test results SM Table S5). Only the HP and Morphological Filters were statistically equal. GrabCut, the segmentation method with the highest median accuracy, was statistical different from every other groups. Therefore, for AlexNet, the best image segmentation method was GrabCut.

Regarding the optimizers applied to AlexNet architecture, although RMSProp provided the highest median accuracy (70.1%), Adagrad achieved the highest accuracy (95.4%). No significant difference between optimizers could be determined (SM Table S6), thus, to determine the best combination for AlexNet, the best-performing segmentation (GrabCut) and optimizer (Adagrad) were selected as they provided both the highest median and maximum accuracies.

For 3ConvLayer, the highest median accuracy (71.8%) was reached when the HP filter was applied to the original images, followed by GrabCut with 71.3% median accuracy (Fig. 4). Nevertheless, the maximum accuracy (94.5%) was achieved when 3ConvLayer was used with GrabCut. Similar to AlexNet, while either using no segmentation or Watershed segmentation, the network cannot be reliably trained (median accuracies of 50.0% each).

There was a difference in accuracy for the image segmentation methods (KW *p*-value: 1.70 $10^{-6}$, PW results SM Table S7). There is no significant difference between None and Watershed and None between Canny, GrabCut and both HP and Morphological Filters. As GrabCut provides the best maximum accuracy, it was chosen as the best segmentation technique for 3ConvLayer.

Regarding optimizers for 3ConvLayer, the highest median accuracies were achieved with the Adam optimizer (66.3%) and RMSProp (63.8%). The Adagrad optimizer was ineffective (median accuracy 50.0%; highest accuracy 54.1%). There was a significant difference of accuracy between optimizers (KW *p*-value: 6.36 $10^{-10}$, PW test results SM Table S8).

The Adagrad optimizer was significantly different from all three other optimizers, but there is no significant difference between Adam, RMSProp and SGD. However, RMSProp was chosen as the best optimizer, as it provided the highest accuracy with GrabCut segmentation (94.5%). Thus, for 3ConvLayer the best combination was GrabCut segmentation with the RMSProp optimizer.

For 2ConvLayer network (Fig. 4), the highest median accuracy (86.1%) was achieved with GrabCut segmentation, followed by the Morphological Filter (84.9%). GrabCut also achieved the highest maximum accuracy (93.3%). When no image segmentation technique and when Watershed was used; accuracy >90.0% was achieved for the 2ConvLayer network.

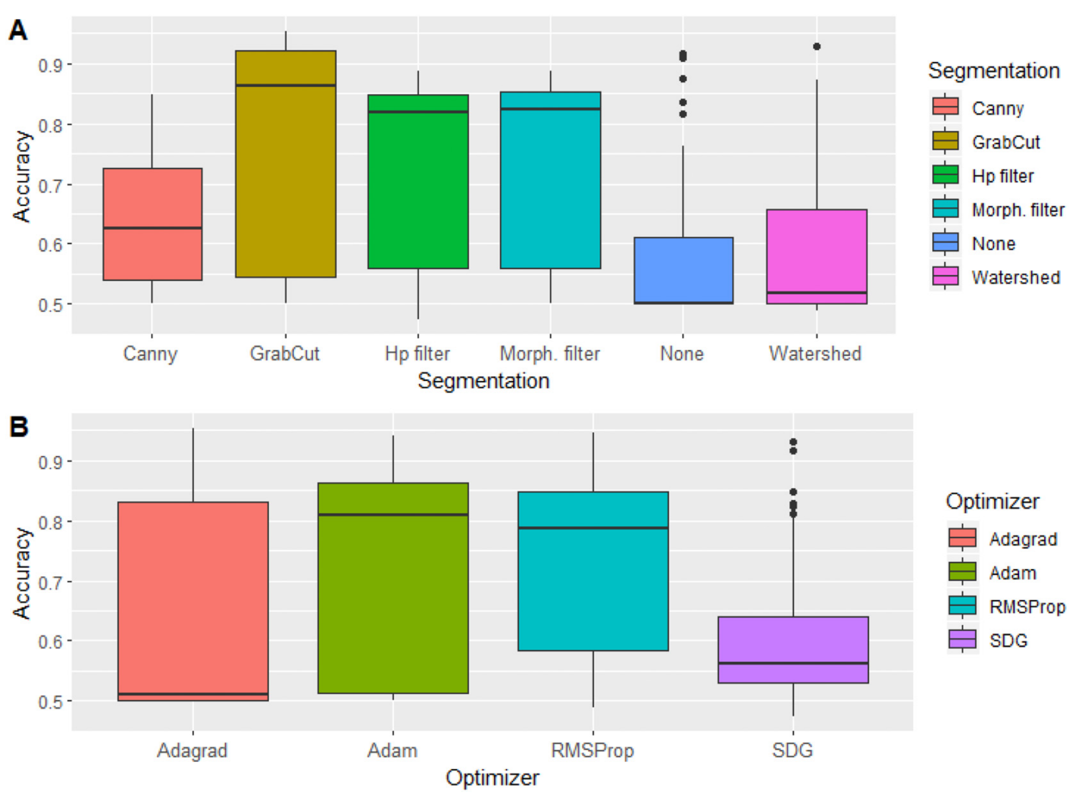


**Fig. 3.** The effect of different segmentation techniques (A) and different optimizers (B) on overall accuracy achieved by different CNN architectures in determining chemically induced morphological changes in *P. agardhii* after 6 h contact time with 80 mg $L^{-1}$ $H_2O_2$.

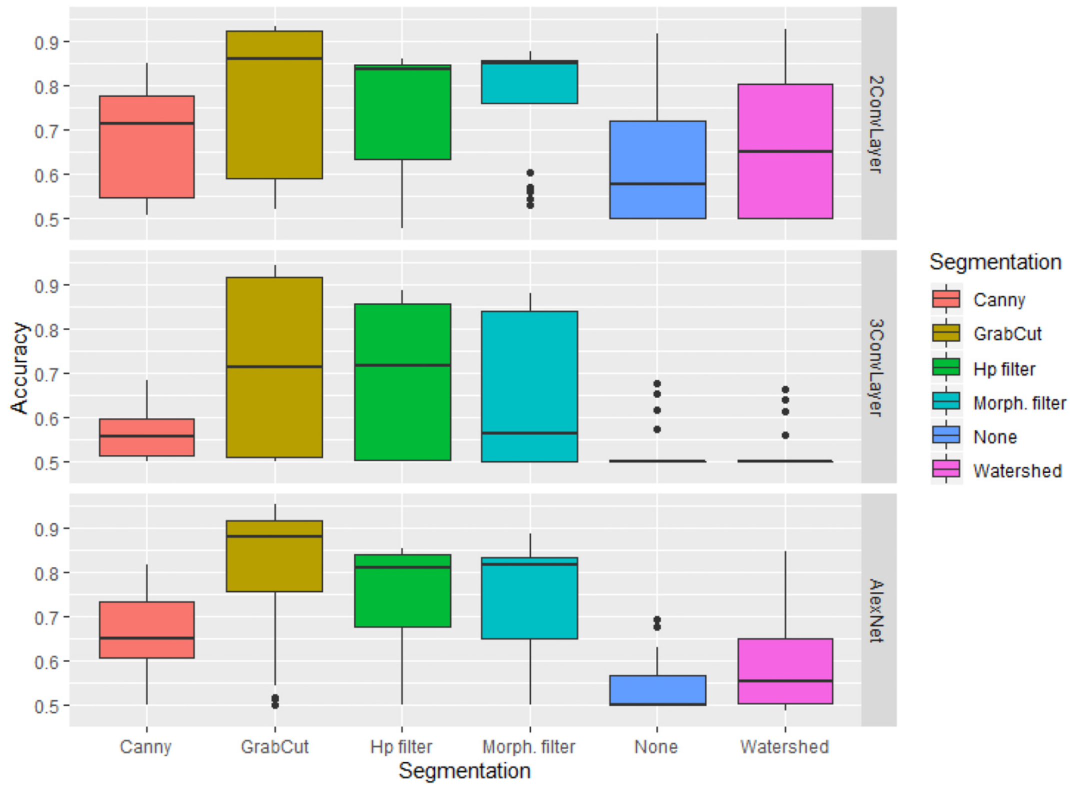


**Fig. 4.** The effect of different segmentation on overall accuracy achieved by each CNN architectures in determining chemically induced morphological changes in *P. agardhii* after 6 h contact time with 80 mg $L^{-1}$ $H_2O_2$.

There was a significant difference between segmentation methods (KW p-value: 2.90 $10^{-5}$, PW test results SM Table S9). No significant difference between Canny, no segmentation and Watershed was detected. There was also no significant difference between the GrabCut and Morphological Filter segmentation techniques. As GrabCut achieved the maximum accuracy for the 2ConvLayer architecture, it was chosen as the best image segmentation technique.

For optimizers, Adam provided the highest median accuracy (84.4%), followed by RMSProp (82.0%). There was significant difference between optimizers (KW p-value: 3.61 $10^{-9}$, PW test results SM Table S10). There was no significant difference between Adam, Adagrad and RMSProp, with only SGD significantly different from all others. However, Adam was selected, as it provided both the highest median and maximum accuracies for the 2ConvLayer architecture.

*3.2.6. Proposing an optimal combination of CNN architecture, segmentation, and optimizer for pattern detection on chemical-stressed P. agardhii*

To determine the optimal combination of CNN architecture, segmentation and optimizer 31 runs were selected where accuracy values were ≥90.0%, to analyse other possible suitable combinations (SM Table S11).

Among the 31 runs, five different combinations were selected to be rerun to analyse the effect of the random division of training, test and validation sets on accuracy (Fig. 5). The selected combinations were: Combination 1 (C1): 2ConvLayer/GrabCut/Adam; Combination 2 (C2): AlexNet/GrabCut/Adagrad; Combination 3 (C3): 3ConvLayer/GrabCut/RMSProp; Combination 4 (C4): 2ConvLayer/None/RMSProp; Combination 5 (C5): 2ConvLayer/None/Adam.

Each of those five combinations was run ten times (SM Table S12). The highest median accuracy (93.3%) was achieved C1, reaching a maximum accuracy of 94.2%. The median accuracy values for both C2 and C3 were 92.7% and, 91.0%, respectively. Although, C4, achieved 92.8% maximum accuracy, this combination had a high standard deviation (0.171), being unable to train (accuracy ~50%) in three out of ten runs. While C5 had the highest standard deviation (0.179), being unable to train in six out ten runs.

There were significant differences between the five combinations (KW *p*-value: 1.29 $10^{-6}$, PW test results SM Table S13), C1 was significantly different from all but C2. Further, there was no significant difference between C4 and C5, the two combinations without image segmentation and the lowest median accuracies (C4: 83.0%; C5: 50.0%).

Although C2 achieved the highest overall accuracy (95.5%), C1 was chosen as the most suitable combination, since it is shallower, has fewer trainable parameters, it could be trained properly earlier than C2 (10 epochs versus 25 epochs, respectively). Moreover, since C1 had the highest median accuracy, it proved to be more reliable than C2, despite the lack of statistical difference between them.

Since many locations (e.g. developing countries) worldwide face a scenario of both occurrence of harmful algal bloom and the lack sophisticated devices for detection of cyanotoxins (e.g. LC/MS) the present study is a ground-breaking step in developing a low cost tool based on image recognition to ensure water safety globally, as we offered a new approach on water treatment quality monitoring. This allows the development of a shallow-CNN-based application for computers or other electronic devices (e.g. smartphones and tablets) which will be able to provide toxin release risk warnings to the operators of different water treatment systems through a single photograph acquired by a simple set-up of microscope and camera.

Having demonstrated that a relatively small amount of cyanobacteria images (2099 before/2099 after $H_2O_2$ exposure), with the appropriate image segmentation technique, is sufficient to train networks like C1, the presented neural network architecture will likely work for other cyanobacterial species. Due to the comparatively simple morphology of cyanobacteria images will present a sufficient level of detail and variation to train the network to detect morphological changes in other cyanobacterial species.

Which means that instead of acquiring costly sophisticated toxin detection equipment for each water treatment plant/system, water utilities

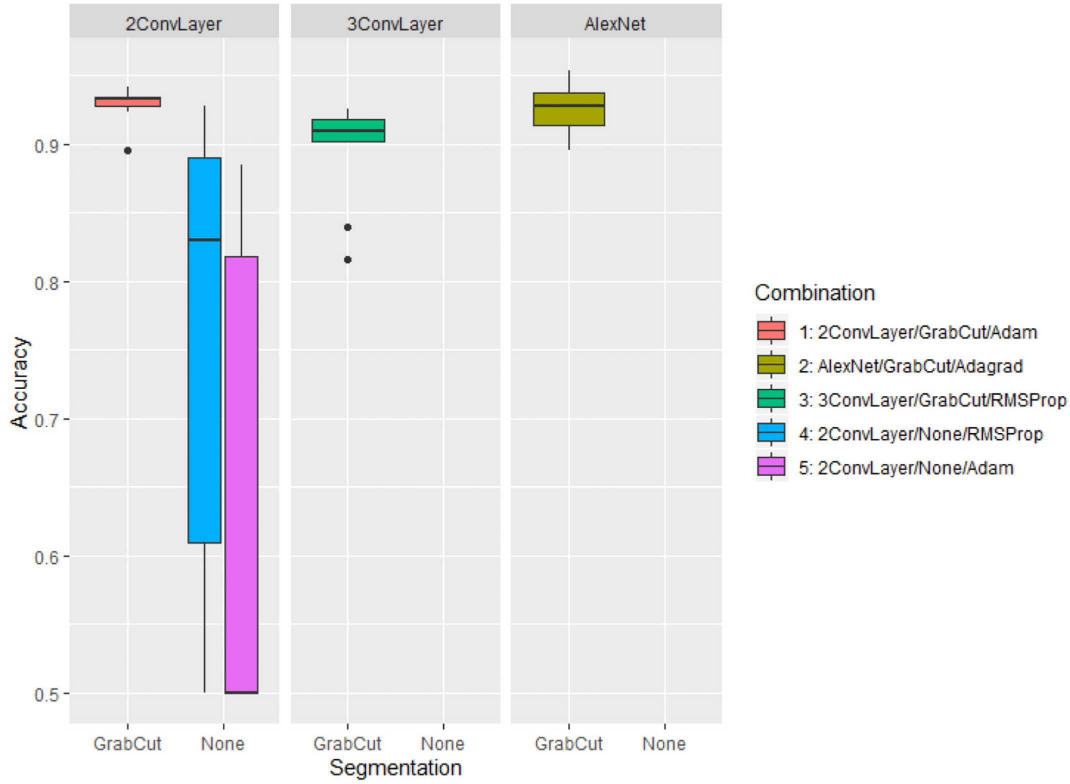


**Fig. 5.** Accuracies achieved by the final five combinations of CNN architecture, image segmentation and optimizer for detection of chemically induced morphological changes in *P. agardhii* after 6 h contact with 80 mg $L^{-1}$ $H_2O_2$.

could train networks for different species of cyanobacteria. This would allow utilities to specifically target known bloom-forming and toxin-producing cyanobacteria species individually for each raw water body. Implementing a routine for micrographics production to detect morphological changes in the required cyanobacteria species through this proposed network as an early warning or an indication of the potential for toxin release into product water.

Such a warning system is crucial to water treatment systems in remote areas, where it might take many hours and even days to collect and prepare samples to perform chromatographic analysis to discover whether there are cyanotoxins in the product water. Such a time lag could endanger public health, as entire populations could potentially consume cyanotoxin present in tap water. Using the proposed system, WTP operators could, in minutes, detect the potential for cell lysis/morphological changes in cyanobacteria species and adjust the treatment operations (especially steps involving chemical oxidation) in order to remove cyanobacteria without compromising the integrity of cells and avoiding consequent toxin release into the product water.

## CRediT authorship contribution statement

**Ismael Carloto:** Conceptualization, Methodology, Validation, Formal analysis, Investigation, Data curation, Visualization, Writing – original draft. **Pamela Johnston:** Conceptualization, Methodology, Validation, Formal analysis, Writing – original draft. **Carlos J. Pestana:** Conceptualization, Writing – review & editing, Supervision. **Linda A. Lawton**: Writing - review & editing, Supervision, Funding acquisition.

## Declaration of competing interest

The authors declare that they have no known competing financial interests or personal relationships that could have appeared to influence the work reported in this paper.

## Acknowledgements

Ismael Carloto would like to acknowledge the Federal Institute of Ceara (IFCE) for granting sabbatical leave and making this research possible. Linda A. Lawton and Carlos J. Pestana would like to acknowledge the Engineering and Physical Sciences Research Council (EPSRC) for funding this research [EP/P029280/1]. As per EPSRC requirements, the data will be made publicly available on the Robert Gordon University's repository, OpenAIR@RGU.

## Appendix A. Supplementary data

Supplementary data to this article can be found online at https://doi.org/10.1016/j.scitotenv.2021.146956.

## References

Baeka, S.-S., Pyo, J., Pachepsky, Y., Park, Y., Ligaray, M., Ahnd, C.-Y., Kim, Y.-H., Chun, J.A., Cho, K.H., 2020. Identification and enumeration of cyanobacteria species using a deep neural network. Ecol. Indic. 115 (106395). https://doi.org/10.1016/j.ecolind.2020.106395.

Barrington, D.J., Ghadouani, A., 2008. Application of hydrogen peroxide for the removal of toxic cyanobacteria and other phytoplankton form wastewater. Environ. Sci. Technol. 42 (23), 8916–8921. https://doi.org/10.1021/es801717y.

Barros, M.U.G., Carloto, I.K.L., Carvalho, S.M.C., Capelo Neto, J., 2017. Impact of filamentous cyanobacteria on the quality of two tropical reservoirs. Braz. J. of Water Resources. 22 (6). https://doi.org/10.1590/2318-0331.011716072.

Bauzá, L., Aguilera, A., Echenique, R., Andrinolo, D., Giannuzzi, L., 2014. Application of hydrogen peroxide to the control of eutrophic lake systems in laboratory assays. Toxins. 6 (9), 2657–2675. https://doi.org/10.3390/toxins6092657.

Canny, J., 1986. A computational approach to edge detection. IEEE T Pattern Anal. 8 (6), 679–698. https://doi.org/10.1109/TPAMI.1986.4767851.

Carloto, I.K.L., Barros, M.U.G., Pestana, C.J., Capelo Neto, J., 2015. Prevalence of paralytic selfish poison-producing *Planktothrix agardhii* and *Cylindrospermopsis raciborskii* in a Brazilian semiarid reservoir. Acta Limnol. Bras. 27 (2), 238–246. https://doi.org/10.1590/S2179-975X5014.

Chen, J.-J., Yeh, H.-H., Tseng, I.-C., 2009. Effect of ozone and permanganate on algae coagulation removal – pilot and bench scale tests. Chemosphere. 74 (6), 840–846. https://doi.org/10.1016/j.chemosphere.2008.10.009.

Cheng, H.D., Jiang, X.H., Sun, Y., Wang, J., 2001. Color image segmentation: advances and prospects. Pattern Recogn. 34, 2259–2281. https://doi.org/10.1016/s0031-3203(00)00149-7.
Chung, K., 1954. On a stochastic approximation method. Ann. Math. Stat. 25, 463–483.
Ciresan, D.C.; Meier, U.; Masci, J.; Gambardella, L.M.; Schmidhuber, J. High-performance neural networks for visual object classification. Technical Report No. IDSIA-01-11. 2011; arXiv:1102.0183.
Daly, R.I., Ho, L., Brookes, J.D., 2007. Effect of chlorination on *Microcystis aeruginosa* cell integrity and subsequent microcystin release and degradation. Environ. Sci. Technol. 41 (12), 4447–4453. https://doi.org/10.1021/es070318s.
Deng, J., Dong, W., Socher, R., Li, L.-J., Li, K., Fei-Fei, L., 2009. Imagenet: a large-scale hierarchical image database. PROC CVPR IEEE, pp. 248–255 https://doi.org/10.1109/CVPR.2009.5206848.
Drabkova, M., Admiraal, W., Marsalek, B., 2007. Combined exposure to hydrogen peroxide and light-selective effects on cyanobacteria, green algae, and diatoms. Environ. Sci. Technol. 41 (1), 309–314. https://doi.org/10.1021/es060746i.
Duchi, J., Hazan, E., Singer, Y., 2011. Adaptive subgradient methods for online learning and stochastic optimization. J. Mach. Learn. Res. 12, 2121–2159. https://doi.org/10.5555/1953048.2021068.
Dunker, S., Boho, D., Waldchen, J., Mader, P., 2018. Combining high-throughput imaging flow cytometry and deep learning for efficient species and life-cycle stage identification of phytoplankton. BCM Ecol. 18 (51). https://doi.org/10.1186/s12898-018-0209-5.
Fan, J., Ho, L., Hobson, P., Brookes, J., 2013. Evaluating the effectiveness of copper sulphate, chlorine, potassium permanganate, hydrogen peroxide and ozone on cyanobacterial cell integrity. Water Res. 47 (14), 5153–5164. https://doi.org/10.1016/j.watres.2013.05.057.
Fan, J., Hobson, P., Ho, L., Daly, R., Brookes, J., 2014. The effects of various control and water treatment processes on the membrane integrity and toxin fate of cyanobacteria. J. Hazard. Mater. 264, 313–322. https://doi.org/10.1016/j.jhazmat.2013.10.059.
Galar, M., Fernandez, A., Barrenechea, E., Bustince, H., Herrera, F., 2012. A review on ensembles for the class imbalance problem: bagging-, boosting-, and hybrid-based approaches. IEEE T. Sys. Man Cyb. C. 42 (4). https://doi.org/10.1109/TSMCC.2011.2161285.
Hobson, P., Dickson, S., Burch, M., Olivia, T., Tsymbal, L., House, J., Brookes, J., Chang, D., Kao, S.-C., Lin, T.-F., Bierlein, K., Little, J., 2012. Alternative and innovative methods for source water management of algae and cyanobacteria. Project Number 4094. Water Research Foundation, Denver, CO.
Huisman, J., Codd, G.A., Paerl, H.W., Ibelings, B.W., Verspagen, J.M.H., Visser, P.M., 2018. Cyanobacterial blooms. Nature Rev. Microb. 16, 471–483. https://doi.org/10.1038/s41579-010-0040-1.
Huo, X., Chang, D.-W., Tseng, J.-H., Burch, M.D., Lin, T.-F., 2015. Exposure of *Microcystis aeruginosa* to hydrogen peroxide under light: kinetic modelling of cell rapture and simultaneous microcystin degradation. Environ. Sci. Technol. 49 (9), 5502–5520. https://doi.org/10.1021/acs.est.5b00170.
Jian, Z., Bai, Y., Chang, Y., Liang, J., Qu, J., 2019. Removal of micropollutants and cyanobacteria from drinking water using $KMnO_4$ pre-oxidation coupled with bioaugmentation. Chemosphere. 215, 1–7. https://doi.org/10.1016/j.chemosphere.2018.10.013.
Kingma, D.P., Ba, J., 2014. Adam: a method for stochastic optimization. arXiv preprint arXiv:1412.6980.
Krizhevsky, A., Sutskever, I., Hinton, G.E., 2012. Imagenet classification with deep convolutional neural networks. Adv. Neur. In. 25, 1097–1105. https://doi.org/10.1145/3065386.
Latifi, A., Ruiz, M., Zhang, C.-C., 2009. Oxidative stress in cyanobacteria. FEMS Microbiol. Rev. 33, 258–278. https://doi.org/10.1111/j.1574-6976.2008.00134.x.
LeCun, Y., Bottou, L., Bengio, Y., Haffner, P., 1998. Gradient-based learning applied to document recognition. P. IEEE. 86 (11), 2278–2324. https://doi.org/10.1109/5.726791.
Li, X., Liao, R., Zhou, J., Leung, P.T., Yan, M., Ma, H., 2017. Classification of morphological similar algae and cyanobacteria using Meuller matrix imaging and convolutional neural networks. Appl. Opt. 56 (23). https://doi.org/10.1364/AO.56.006520.
Matthijs, H.C.; Visser, P.M.; Reeze, B.; Meeuse, J.; Slot, P.C.; Wijn, G.; Talens, R.; Huisman, J. Selective suppression of harmful cyanobacteria in an entire lake with hydrogen peroxide. Water Res. 2012, 46 (5), 1460–72; DOI:https://doi.org/10.1016/j.watres.2011.11.016.
Matthijs, H.C.P., Jančula, D., Visser, P.M., Maršálek, B., 2016. Existing and emerging cyanocidal compounds: new perspectives for cyanobacterial bloom mitigation. Aquat. Ecol. 50, 443–460. https://doi.org/10.1007/s10452-016-9577-0.
Meyer, F., 1992. Color image segmentation. 1992 IEE Conf. Publ, pp. 303–306.
Otsu, N., 1979. A threshold selection method from gray-level histogram. IEEE T. Sys. Man Cyb. 9 (1), 62–66. https://doi.org/10.1109/TSMC.1979.4310076.47.
Panta, G., Yadav, D.P., Gaur, A., 2020. ResNeXt convolution neural network topology-based deep learning model for identification and classification of Pediastrum. Algal Res. 48 (101932). https://doi.org/10.1016/j.algal.2020.101932.
Park, J., Lee, H., Park, C.Y., Hasan, S., Heo, T.-Y., Lee, W.H., 2019. Algal morphological identification in watersheds for drinking water supply using neural architecture search for convolutional neural network. Water. 11 (7), 1338. https://doi.org/10.3390/w11071338.
Pedraza, A., Bueno, G., Deniz, O., Cristobal, G., Blanco, S., Borrego-Ramos, M., 2017. Automated diatom classification (part B): a deep learning approach. App. Science. 7 (460). https://doi.org/10.3390/app7050460.
Pietsch, J., Bornmann, K., Schmidt, W., 2002. Relevance of intra- and extracellular cyanotoxins for drinking water treatment. Acta Hydrochim. Hydrobiol. 30 (1), 7–15. https://doi.org/10.1002/1521-401X(200207)30:1<7::AID-AHEH7>3.0.CO;2-W.
Qian, P., Zhao, Z., Liu, H., Wang, Y., Peng, Y., Hu, S., Zhang, J., Deng, Y., Zeng, Z., 2020. Multi-target deep learning for algal detection and classification. Eng. Med. Biol. Soc. Ann., 1954–1957. arxiv.org/abs/2005.03232.
Rippka, R., Josette, D., Waterbury, J.B., Herdman, M., Roger, Y.S., 1979. Generic assignments, strain histories and properties of pure cultures of cyanobacteria. J. Gen. Microbiol. 111 (1), 1–61. https://doi.org/10.1099/00221287-111-1-1.
Rother, C., Kolmogorov, V., Blake, A., 2004. "GrabCut" interactive foreground extraction using iterated graph cuts. ACM T. Graphic. 23 (3), 309–314. https://doi.org/10.1145/1015706.1015720.
Sarigul, M., Ozyildirim, B.M., Avci, M., 2019. Differential convolutional neural network. Neural Netw. 116, 279–287. https://doi.org/10.1016/j.neunet.2019.04.025.
Steynberg, M.C., Guglielmi, M.M., Geldenhuys, J.C., Pieterse, A.J.H., 1996. Chlorine and chlorine dioxide: pre-oxidants used as algicide in potable water plants. J. Water Supply Res. T. 45 (4), 162–170.
Tang, N., Zhou, F., Gu, Z., Zheng, H., Yu, Z., Zheng, B., 2018. Unsupervised pixel-wise classification for Chaetoceros image segmentation. Neurocomputing. 318, 261–270. https://doi.org/10.1016/j.neucom.2018.08.064.
Tieleman, T., Hinton, G., 2012. Lecture 6.5 - RMSProp. Technical Report for COURSERA: Neural Networks for Machine Learning.
Wang, Z., Li, D., Qin, H., Li, Y., 2012. An integrated method for removal of harmful cyanobacterial blooms in eutrophic lakes. Environ. Pollut. 160 (1), 34–41. https://doi.org/10.1016/j.envpol.2011.09.003.
Wang, X., Ma, B., Bai, Y., Lan, H., Liu, H., Qu, J., 2018. The effects of hydrogen peroxide pre-oxidation on ultrafiltration membrane biofouling alleviation in drinking water treatment. J. Environ. Sci. (China) 73, 117–126. https://doi.org/10.1016/j.jes.2018.01.020.
Westrick, J., Szlag, D., Southwell, B., Sinclair, J., 2010. A review of cyanobacteria and cyanotoxins removal/inactivation in drinking water treatment. Anal. Bioanal. Chem. 397, 1705–1714. https://doi.org/10.1007/s00216-010-3709-5.
Yang, Z., Buley, R.P., Fernandez-Figueroa, E., Barros, M.U.G., Rajendran, S., Wilson, A.E., 2018. Hydrogen peroxide treatment promotes chlorophytes over toxic cyanobacteria in a hypertrophic aquaculture pond. Environ. Pollut. 240, 590–598. https://doi.org/10.1016/j.envpol.2018.05.012.
Ying, T., 2016. GPU-based Parallel Implementation of Swarm Intelligence Algorithms. Morgan Kaufmann, Massachusetts, USA https://doi.org/10.1016/C2015-0-02468-6.
Zamyadi, A., Ho, L., Newcombe, G., Daly, R.I., Burch, M., Baker, P., Prevost, M., 2010. Release and oxidation of cell-bound saxitoxins during chlorination of *Anabaena circinalis* cells. Environ. Sci. Technol. 44 (23), 9055–9061. https://doi.org/10.1021/es102130b.
Zheng, H., Wang, N., Yu, Z., Gu, Z., Zheng, B., 2017. Robust and automatic cell detection and segmentation from microscopic images of non-setae phytoplankton species. IET Image Process. 11 (11), 1077–1085. https://doi.org/10.1049/iet-ipr.2017.0127.
Zhou, Q., Li, L., Huang, L., Guo, L., Song, L., 2018. Combining hydrogen peroxide addition with sunlight regulation to control algal blooms. Environ. Sci. Pollut. Res. Int. 25 (3), 2239–2247. https://doi.org/10.1007/s11356-017-0659-x.